Lipid droplets are central organelles for meiosis II progression during yeast sporulation

Tzu-Han Hsu[a], Rey-Huei Chen[a], Yun-Hsin Cheng[b], and Chao-Wen Wang[b,*]
[a]Institute of Molecular Biology and [b]Institute of Plant and Microbial Biology, Academia Sinica, Nankang, Taipei 11529, Taiwan

ABSTRACT **Neutral lipids, predominantly triacylglycerol (TAG) and sterol ester, are stored within the cellular organelles termed lipid droplets (LDs). Although it is believed that the major function of LDs is to supply the cell with energy and membranes, little is known about the cellular events directly involving LDs and their contents. In this study, we provide cytological evidence that LDs form direct contacts with the prospore membrane (PSM) that is synthesized de novo during meiosis II to sequester the dividing nuclei in sporulating yeast. Lipidomic analyses indicate that TAG lipolysis releases free fatty acids at a time that correlates well with meiosis II progression, concomitant with phospholipid remodeling. Mutants lacking TAG or impaired of TAG hydrolysis show spore wall assembly defects, supporting a role for TAG and/or its metabolites in spore wall morphogenesis. Not only does LD integrity influence spore wall assembly, LDs are also essential for other aspects of spore development. Yeast cells lacking LDs are severely defective in PSM growth and organization and display disrupted spindles, producing dead spores or even failing to form spores. Together these results link LD physiology directly to a unique membrane morphogenesis process critical for development.**

Monitoring Editor
Howard Riezman
University of Geneva

Received: Jun 7, 2016
Revised: Nov 15, 2016
Accepted: Dec 2, 2016

INTRODUCTION

Lipid droplets (LDs) are conserved neutral lipid storage organelles in eukaryotic cells (Walther and Farese, 2012; Wang, 2015). Formation of LDs requires a coupling of neutral lipid synthesis by enzymes that catalyze neutral lipid production in the endoplasmic reticulum (ER) and a complex interplay of ER proteins and lipids at a specific ER subdomain for LD assembly. LDs eventually bulge out from the outer leaflet of the ER, and their characteristic structure contains a phospholipid monolayer surrounding a neutral lipid core. LDs have been implicated in diverse cellular functions, such as modulation of lipid metabolism, protein quality control, and pathogenesis. The storage lipids within LDs provide resources that can be used by cells as fuels, membrane building blocks, and signaling molecules. However, cellular events underlying the demand for LDs and their contents are poorly understood.

In response to a lack of nitrogen and fermentable carbon sources, diploid yeast cells exit the mitotic cell cycle and enter meiosis, leading to formation of four haploid spores—the equivalent of gametes—in the cytoplasm of mother cells. This process is known as sporulation (Neiman, 2011). The hallmark of meiosis II in sporulating budding yeast is the biogenesis of a double-membrane vesicle termed the prospore membrane (PSM; Neiman, 1998). The structure forms de novo from the cytoplasmic face of each of the four spindle pole bodies (SPBs) derived from previous divisions at meiosis I and II (Moens and Rapport, 1971; Knop and Strasser, 2000). The expansion and growth of the PSM must be tightly controlled because it functions to sequester the four dividing nuclei along with a portion of cytoplasm to form four spores, also known as tetrads. After closure of the PSM, spore wall biogenesis begins with expansion of the lumen of the PSM, where it serves as the site for spore wall deposition. The mature spore contains four distinct layers of spore wall, from the innermost mannoproteins, β-glucan and chitosan, to the

This article was published online ahead of print in MBoC in Press (http://www.molbiolcell.org/cgi/doi/10.1091/mbc.E16-06-0375) on December 8, 2016.

C.-W.W. conceived and designed the experiments. All of the authors performed the experiments and analyzed the data. C.-W.W. and R.-H.C. contributed reagents, materials, and analysis tools. C.-W. W. interpreted the data and wrote the manuscript. R.-H.C. commented on the manuscript.

*Address correspondence to: Chao-Wen Wang (cwwang02@gate.sinica.edu.tw).

Abbreviations used: CFW, calcofluor white; EM, electron microscopy; ER, endoplasmic reticulum; FA, fatty acid; LC, liquid chromatography; LD, lipid droplet; MOP, meiosis II outer plaque; PA, phosphatidic acid; PC, phosphatidylcholine; PE, phosphatidylethanolamine; PI4,5-P2, phosphatidylinositol 4,5-bisphosphate; PLD, phospholipase D; PSM, prospore membrane; SE, sterol ester; SPB, spindle pole body; SPO, sporulation medium; TAG, triacylglycerol.

outermost, dityrosine (Klis *et al.*, 2002; Coluccio *et al.*, 2004; Lesage and Bussey, 2006). The outer PSM is degraded halfway during the spore wall assembly, whereas the inner PSM eventually develops into the new plasma membrane of the spore.

Precursor PSM is nucleated by the docking and fusion of post-Golgi vesicles at an SPB-associated cytoplasmic protein complex termed the meiosis II outer plaque (MOP; Nakanishi *et al.*, 2004; Riedel *et al.*, 2005). While anchored on the MOP, the PSM rapidly grows and eventually engulfs the nuclei. The growth and organization of the PSM require a number of factors. One essential player is Spo14, the phospholipase D (PLD) that catalyzes conversion of phosphatidylcholine (PC) to phosphatidic acid (PA; Rose *et al.*, 1995; Rudge *et al.*, 1998; Nakanishi *et al.*, 2006). Recruitment and activation of Spo14 on the PSM require sufficient levels of phosphatidylinositol 4,5-bisphosphate (PI4,5-P2; Rudge *et al.*, 1998, 2004; Sciorra *et al.*, 1999), indicating that lipid remodeling is coupled to growth and organization of the PSM. Sporulating cells lacking Vps13 display a PSM morphogenesis defect, resulting from reduced levels of phosphatidylinositol 4-phosphate, PI4,5-P2, and PA (Park and Neiman, 2012). Vps13 is translocated from the endosome to the PSM, where it works cooperatively with Spo71 to regulate PSM elongation and closure (Parodi *et al.*, 2012; Park *et al.*, 2013). In addition to a flux of various lipids, proper PSM growth also relies on two protein complexes. The leading-edge complex resides on the lip of the growing PSM, and its breakdown during meiotic exit allows membrane closure (Moreno-Borchart *et al.*, 2001; Maier *et al.*, 2007; Diamond *et al.*, 2009). The septin complex forms sheets or bars and associates with the PSM (Fares *et al.*, 1996; Tachikawa *et al.*, 2001), perhaps as scaffolds for membrane morphogenesis.

An association between LDs and the PSM was observed in several early electron microscopy (EM) studies (Lynn and Magee, 1970; Guth *et al.*, 1972). More recent evidence indicates that a pool of LDs is recruited to the outside of the PSM and that various proteins localized to this subpopulation of LDs may directly contribute to spore wall morphogenesis (Lin *et al.*, 2013). In addition, these LDs are enriched in certain lipases and a homologue of the Sec 14 phosphatidylinositol transfer protein Sfh3/Pdr16, which is implicated in coupling phosphoinositide signaling with LD homeostasis during PSM formation (Ren *et al.*, 2014). In this study, we combine live-imaging, ultrastructural micrographs, genetics, and lipidomic analyses to comprehensively investigate when and how LDs associate with the PSM and their physiological effect. We find that triacylglycerol (TAG) hydrolysis and LD integrity are crucial factors for proper spore wall assembly. Strikingly, LD-deficient cells form abnormally small, branched, and irregular PSM that often fail in membrane nucleation and expansion. In addition, the mutant is defective in meiotic spindle organization and produces inviable spores. We propose that LDs may orchestrate PSM morphogenesis through their physical contact with the PSM.

RESULTS

LDs were relocalized from the surface of vacuoles to the forming PSM

Recent studies suggested that recruitment of a distinct class of LD proteins to the spore wall is required for spore formation and spore wall assembly (Lin *et al.*, 2013), raising the possibility that LDs play an active role during sporulation. To define the physiological importance of LDs, both spatially and temporally, during diploid yeast sporulation, we choose the strain SK1, which has been routinely used for synchronous meiosis studies. The most crucial membrane morphogenesis event in sporulating yeast cells is de novo synthesis of the PSM from the MOP during meiosis II to eventually engulf the entire nucleus, leading to the formation of tetrads. Biogenesis of the PSM requires developmentally regulated hydrolysis of PC to PA, catalyzed by phospholipase D (Rose *et al.*, 1995; Rudge *et al.*, 1998). Thus the amphipathic helix of Spo20 (residues 51–91), which binds to PA-rich membranes in vivo, has been widely used as a PSM marker (Nakanishi *et al.*, 2006).

Using a microfluidic device, we imaged LDs stained with the neutral lipid-binding dye BODIPY 493/503 by time-lapse microscopy. The LDs in sporulating yeast were highly dynamic and transitioned from a dispersed to a clustered pattern during spore formation (Figure 1A). LDs are known to associate closely with the ER and vacuole in yeast (Jacquier *et al.*, 2011; Wang *et al.*, 2014b). By imaging the vacuolar marker Vph1–green fluorescent protein (GFP), we found that vacuoles occupied most of the cell volume, particularly before meiosis II, when the Spo20-BFP signal was weak and diffused (Figure 1B, left). At this stage, nuclear ER labeled with Elo3-GFP showed a dumbbell-shaped structure at the cell periphery (Figure 1B, right), and most LDs labeled with Erg6-mCherry localized to the surface of the vacuole. However, during PSM biogenesis, LDs no longer distributed throughout the surface of the vacuole but instead clustered toward the nucleus (Figure 1B). The LD staining gradually became diffused along the expanding PSM, whereas a small portion of the vacuole and LDs, together with the nuclei, was enclosed by the PSM and subsequently found in each of the tetrads. Finally, vacuoles that were pulled away by the forming tetrads eventually burst (Eastwood and Meneghini, 2015). Consistent with previous findings suggesting two distinct populations of LDs in sporulating yeast cells (Ren *et al.*, 2014), the LD protein Pet10 was associated with only the LDs inside but not those outside of the PSM, whereas the LD protein Erg6 was found in both pools (Figure 1C). Taken together, these imaging results supported an LD distribution precisely regulated toward spore formation in space and time during meiosis I and II (Figure 1D).

LDs docked on the surface of forming PSM and then shrunk

We next performed freeze substitution EM to further determine how LDs can interact with the PSM. In yeast, LDs form and associate mostly with the ER (Figure 2A), and the ER–LD contact site is organized by the seipin protein complex (Szymanski *et al.*, 2007; Fei *et al.*, 2008; Wang *et al.*, 2014a; Grippa *et al.*, 2015). We observed LD association with the surface of the vacuole before meiosis II (Figure 2A) and substantial vesicle accumulation near the precursor membrane at the electron-dense MOP at the onset of meiosis II (Figure 2Ba and Supplemental Figure S1). Of interest, we found that LDs docked on the PSM immediately after the precursor PSM appeared (Figure 2Bb). During expansion and elongation of the PSM, a number of LDs were recruited to its surface (Figure 2Bc and Supplemental Figure S1) and the forming PSM-sequestered organelles, such as mitochondria, LDs, and vacuoles (Figure 2B).

The ultrastructural evidence provided further interesting insights. The PSM-docked LDs looked differently from those associated with the ER and vacuole or those sequestered by the PSM. The PSM-docked LDs appeared to shrink and became electron-dense during expansion of the PSM (Figure 2C). By contrast, the electron-translucent LDs that were enclosed by the PSM were larger than the PSM-docked LDs (Figure 2, C and D). In addition, the internal LDs associated with the perinuclear ER via a small contact site, distinct from the external LDs, which often contacted the PSM with a larger surface area (Figure 2C), indicative of a unique mechanism for association of LDs with the PSM. Taken together, this cytological evidence supports the view that LDs were recruited to the expanding PSM and gradually diminished as the PSM grew during meiosis II. In

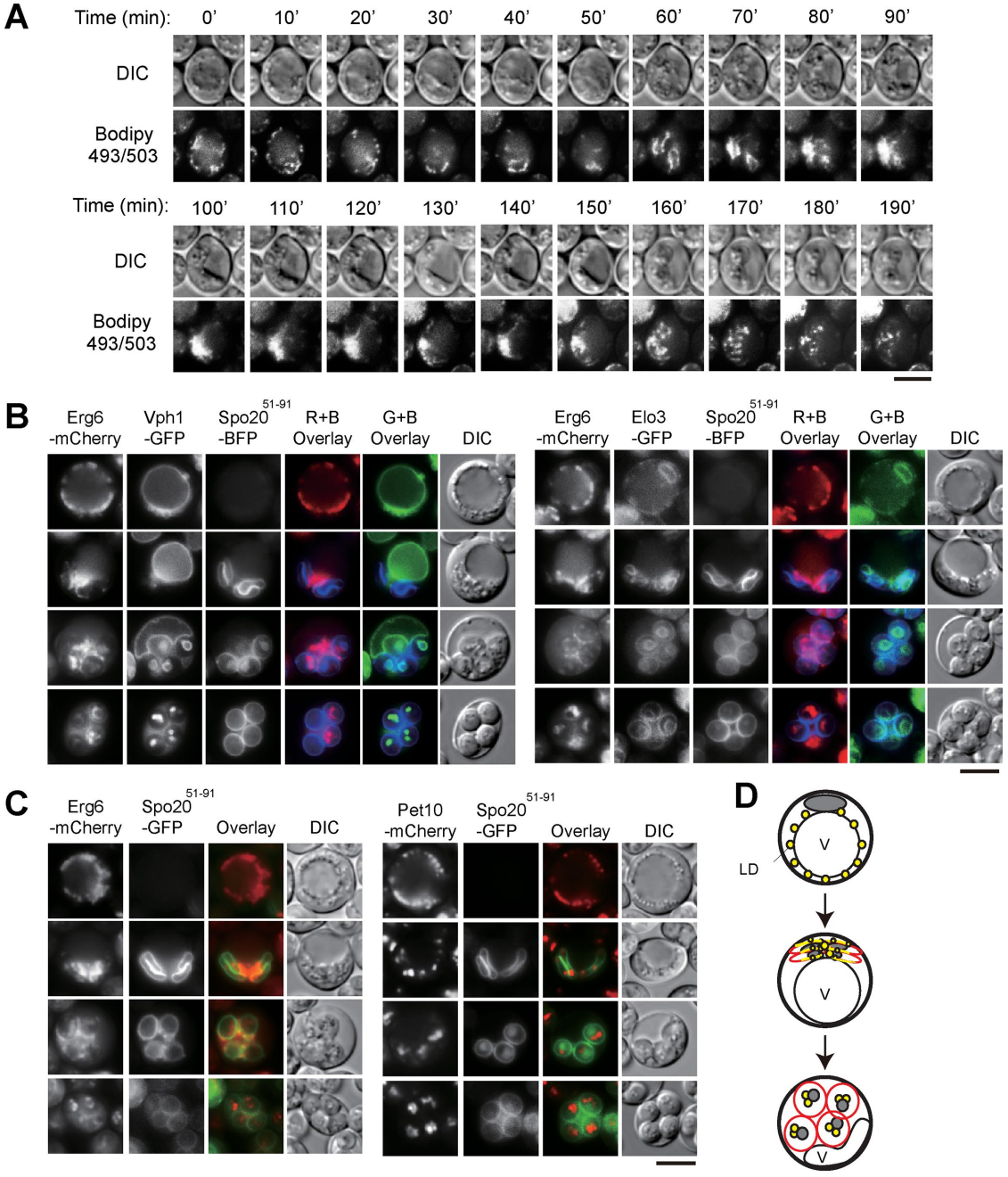

FIGURE 1: Overview of LD dynamics during meiosis I and II. (A) Wild-type cells expressing Spo20 (51-91)-GFP grown in SPO for 8 h were subjected to BODIPY 493/503 staining followed by fluorescence microscopy using the DeltaVision system connected with the CellAsic chamber microfluidic device. Images were taken every 10 min by time lapse. Scale bar, 5 μm. (B) Sporulating cells at different stages expressing Erg6-mCherry (LD), Vph1-GFP (vacuole), or Elo3-GFP (ER) and Spo20 (51-91)-BFP (PSM), as indicated, were subjected to fluorescence microscopy. Scale bar, 5 μm. (C) Sporulating cells at different stages expressing LD protein Erg6-mCherry or Pet10-mCherry and the PSM marker Spo20 (51-91)-GFP, as indicated, were subjected to fluorescence microscopy. Scale bar, 5 μm. (D) LD dynamics during sporulation. LDs (yellow) dispersed along the vacuole surface during meiosis I relocalized to a cluster around the dumbbell-shaped nucleus (gray) during meiosis II when the PSMs (red) start to form. Some LDs appeared to traffic from the cluster to associate with the four forming PSMs, whereas other LDs were enclosed in the four spores by the PSMs. V, vacuole.

addition, these structural differences may reflect lipolysis of LDs when they are associated with the PSM.

LD lipolysis and lipid remodeling occurred during meiosis II

Under our experimental conditions, the wild-type SK1 cells in the sporulation medium (SPO) consistently began DNA replication at ~6 h and entered meiosis II at ~10–12 h (Figure 3A). To gain insights into LD lipolysis, we next performed liquid chromatography/mass spectrometry (LC/MS) followed by lipidomic analysis on wild-type cells shifted to SPO for 0, 4, 8, 12, or 16 h, examining lipid profile changes during sporulation. Intriguingly, TAG profile displayed a reduction of lower–molecule weight species concomitant with

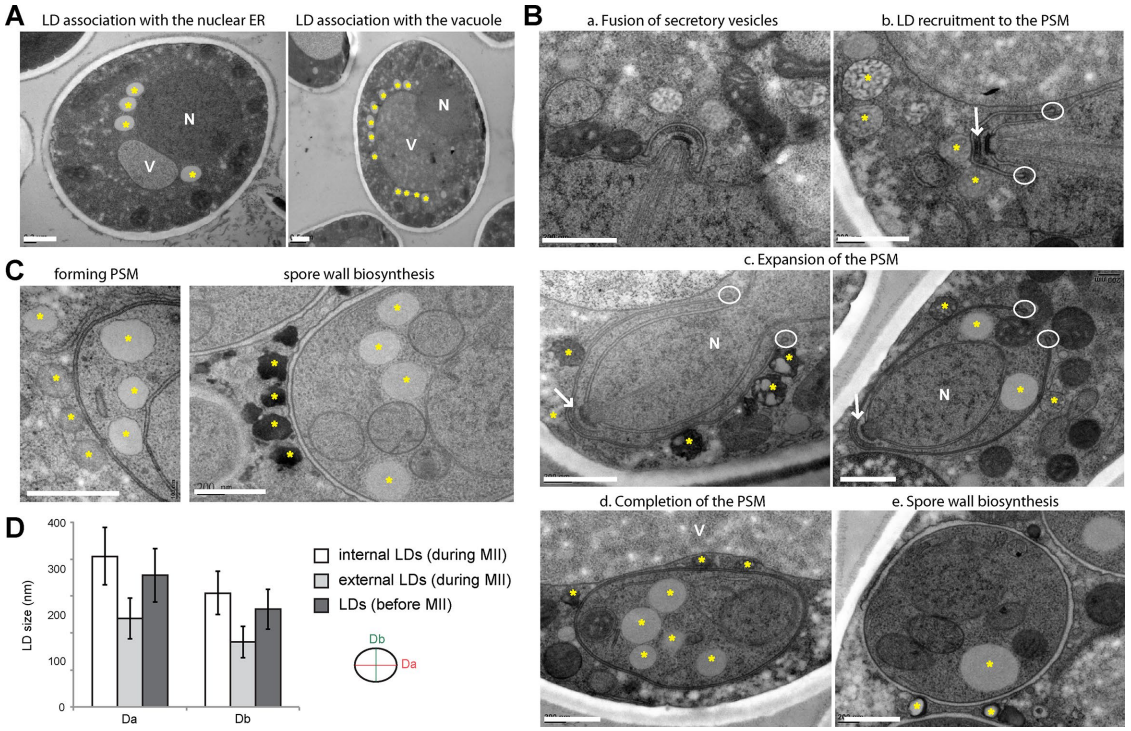

FIGURE 2: Ultrastructure of LDs during yeast sporulation. (A) Wild-type cells grown 12 h in SPO were subjected to freeze-substitution EM. Cells were at the stage prior to meiosis II. Yellow asterisks denote LDs. N, nucleus. V, vacuole. Scale bar, 0.5 µm. (B) Wild-type cells grown in SPO undergoing meiosis II. White arrow depicts MOP. White oval depicts leading-edge complex. Scale bar, 0.5 µm. (C) Comparison of LDs associated with the PSM during early (left) and late (right) stages. Right, spore wall synthesis had begun, but the outer PSM degradation had not yet occurred. Scale bar, 0.5 µm. (D) Quantification of sizes of LDs that were docked on (external) or enclosed by (internal) the forming PSM (during meiosis II, defined by the presence of unsealed PSM) and the LDs in sporulating cells before meiosis II (defined by no PSM appearance). We measured only center sections of LDs that display a sharp monolayer outline in our EM results. The diameter of LDs was determined as indicated. Data presented as mean ± SD (n = 100).

increasing higher–molecular weight species (Figure 3B and Supplemental Figure S2). Most major species of TAG increased during 0–8 h in SPO (Figure 3B and Supplemental Figure S2), when cells were undergoing DNA replication and entering meiosis I. During this period, unsaturated fatty acids (FAs; 16:1 and 18:1) instead of saturated FAs (16:0 and 18:0) decreased, which may indicate a selective consumption of these free FAs to provide fuel or a selective recycling of these FAs for storage as TAG via FA acylation. Consistent with the latter notion, TAG species with double bonds increased significantly in the lipidomics profile during the first 8 h (Figure 3B and Supplemental Figure S2). A reduction of TAG levels occurred at 12 h in SPO, when most SK1 diploid cells entered meiosis II, indicative of lipolysis. The lipidome also revealed a drastic reduction of higher–molecular weight TAG species at 12 h in SPO (Figure 3B and Supplemental Figure S2). This decrease in TAG occurred in parallel with a restoration of free FAs levels, particularly the unsaturated FA 18:1. Unlike those of FA 16:1, which decreased continuously during sporulation, levels of FA 18:1 were maintained after their restoration from meiosis II, at least during 12–16 h in SPO.

We next analyzed the meiotic lipidome for phospholipids and found that PA levels among all phospholipids were significantly upregulated, particularly at meiosis II (Figure 3C and Supplemental Figure S2), consistent with the previously established role of PLD activity for sporulation (Nakanishi *et al.*, 2006). The reduction of lower–molecular weight and increase of higher–molecular weight species during sporulation were also seen with several types of phospholipids, such as PC, phosphatidylethanolamine (PE), and phosphatidylinositol. In addition, some phospholipids changed in abundance at specific stages, such as during the transition from meiosis I to II, and a subset of lysophospholipids and phospholipids appeared to accumulate at times corresponding to meiosis II (Figure 3C and Supplemental Figure S2). This raised the possibility that these particular lipid species might be actively involved in PSM growth or lipid signaling at that stage.

LD lipolysis is required for proper spore wall assembly

As a storage organelle, LDs store two major neutral lipids, TAG and sterol ester (SE). We next investigated the contributions of the two major neutral lipids during LD lipolysis in meiosis II. Yeast cells lacking Are1 and Are2 synthesized TAG but not SE (ΔSE), whereas cells lacking Dga1 and Lro1 accumulated SE but lacked TAG (ΔTAG). We found that both ΔSE and ΔTAG cells showed reduced sporulation efficiency and produced fewer spores (triad, dyad, and monad) than the wild-type cells (Figure 4A). Ultrastructural evidence revealed a higher frequency of irregular internuclear membrane space and giant mitochondria in the ΔSE and ΔTAG mutants, whereas the fine structures of the forming PSM and spore wall in the ΔTAG and ΔSE mutants did not seem to be affected as analyzed by EM (Figure 4, B and C). However, examining the mutant spores stained with the chitin/chitosan-binding dye calcofluor white (CFW) and the chitosan-specific dye eosin Y, as well as by examining dityrosine fluorescence, we found that ΔTAG spores showed reduced eosin Y staining, and

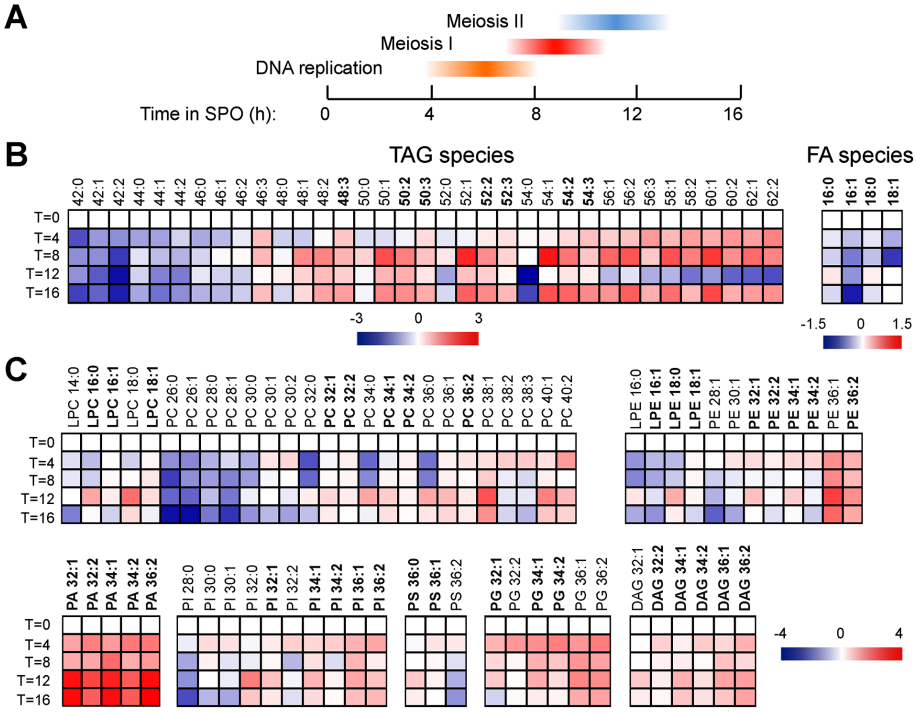

FIGURE 3: A meiotic lipidome reveals TAG lipolysis at meiosis II. (A) Diagram of the sporulation events upon shifting to SPO under our experimental conditions. (B) The abundance of indicated lipid species at indicated time point compared with that at time zero. The $\log_2$-fold change of TAG and FA species at indicated sporulation time points is displayed by the heat map. The abundant lipid species in each category is shown in bold. The relative intensity of each of the lipids is given in Supplemental Figure S2. (C) As described for B, except that levels of various lysophospholipids, phospholipids, and diacylglycerol are compared.

about half of the spores also displayed impaired dityrosine fluorescence (Figure 4D), indicative of spore wall assembly defects. By contrast, ΔSE mutants displayed a staining pattern similar to that of the wild type. Further analyses of the distribution of chromosome mass labeled with Htb2-GFP indicated that chromosomal DNA was well segregated into each of the four spores formed within the ΔTAG and ΔSE mutants (Figure 4E), and the two mutants, like the wild type, produced viable spores as judged by random tetrad dissection (Figure 4F). Thus TAG stored within LDs contributes to proper spore wall morphogenesis without affecting spore viability.

To tackle the role of TAG lipolysis during meiosis II, we then asked whether cells lacking the known LD-localized TAG lipases are defective in spore wall assembly as in the ΔTAG mutants. Consistent with this notion, we found that *tgl3*Δ and *tgl4*Δ but not other known TAG lipase mutants were impaired in their spore wall pattern (Figure 5A). These mutants showed much-reduced eosin Y staining, indicative of aberrant chitosan layer, and failed to synthesize the outer dityrosine layer. Intriguingly, spore wall synthesized in a population of the two mutants was also stained with CFW, which suggests a leakage of their mother cell ascus. Similar to ΔTAG cells, these lipolysis mutant cells segregated their chromosomes properly (Figure 5B) and formed viable spores (Figure 5C). Thus we conclude that LD lipolysis, likely activated by the two TAG lipases Tgl3 and Tgl4 during meiosis II, contributes to spore wall biogenesis in yeast.

The TAG lipase Tgl3 has been reported to catalyze lyso-PE and lyso-PA conversion to PE and PA, respectively. Intriguingly, the acyltransferase, rather than the lipase, activity of Tgl3 is crucial for sporulation (Rajakumari and Daum, 2010). We next analyzed the lipidome of *tgl3*Δ mutants and found that *tgl3*Δ mutants indeed accumulated several fold of TAG compared with wild type (Figure 5D). However, the FA level at 12 h in SPO appeared unaffected, suggesting a redundant role of other lipases to maintain lipid homeostasis in *tgl3*Δ during meiosis II. Although the phospholipid-remodeling pattern in the *tgl3*Δ mutants was similar to that in the wild type during 8–12 h in SPO, the abundance of a subset of phospholipids, such as PE36:2, PA32:1, and PA34:1, was specifically affected at meiosis II (Figure 5E). Thus we consider the possibility that these lipids, which are probably derived from or were affected by TAG lipolysis, are candidates involved in PSM organization for subsequent spore wall morphogenesis. Alternatively, LDs bring LD-localized proteins, such as those found in the pool of LDs associated with the PSM (Lin *et al.*, 2013), and stimulate their functions via LD lipolysis.

Fld1/Ldb16 complex required for LD assembly is needed for spore wall biogenesis

To explore the integrity of LDs for spore development, we next asked whether the yeast seipin complex known to organize the ER–LD contact site for LD assembly is needed for sporulation. Yeast cells deficient in Fld1 or Ldb16 had aberrant LDs, either supersized or small and clustered (Szymanski *et al.*, 2007; Fei *et al.*, 2008; Wang *et al.*, 2014a). These cells also exhibited LD protein distribution defects, with levels of many major LD proteins either reduced or enhanced on the LD surface (Wang *et al.*, 2014a; Grippa *et al.*, 2015). We found that the *fld1*Δ and *ldb16*Δ diploid strains sporulated as efficiently as the wild type (Figure 6A) but produced more triads and dyads (Figure 6B). The LD marker Erg6-GFP, which normally distributed into two distinct populations of LDs during meiosis II, was absent in the internal populations of LDs in both *fld1*Δ and *ldb16*Δ cells (Figure 6C). Moreover, Pet10-mCherry, which was associated largely with LDs inside the spores, was either excluded from internal LDs or found in both pools of LDs inside and outside the spores in both *fld1*Δ and *ldb16*Δ cells (Figure 6C). Thus the LD protein distribution defects were also seen in the LD assembly mutants during sporulation.

Next we performed spore wall staining analyses for *fld1*Δ and *ldb16*Δ cells. The results indicated that the two LD assembly mutants displayed a disrupted chitosan layer as revealed by reduced eosin Y fluorescence and lacked or had an uneven outer dityrosine layer (Figure 6D). The LD assembly defect did not affect chromosome segregation and spore viability as judged by Htb2-GFP pattern and random tetrad dissection assay (Figure 6, E and F). Thus LD integrity is important for spore wall assembly but not spore viability during sporulation. The altered distribution of LD proteins might contribute to the spore wall defects through their functions in spore wall assembly or regulation of lipolysis.

Cells lacking LDs displayed various PSM organization and chromosome segregation defects

The LD-deficient quadruple mutant did not synthesize TAG and SE and thus lacked LDs. The quadruple mutant, like all other strains

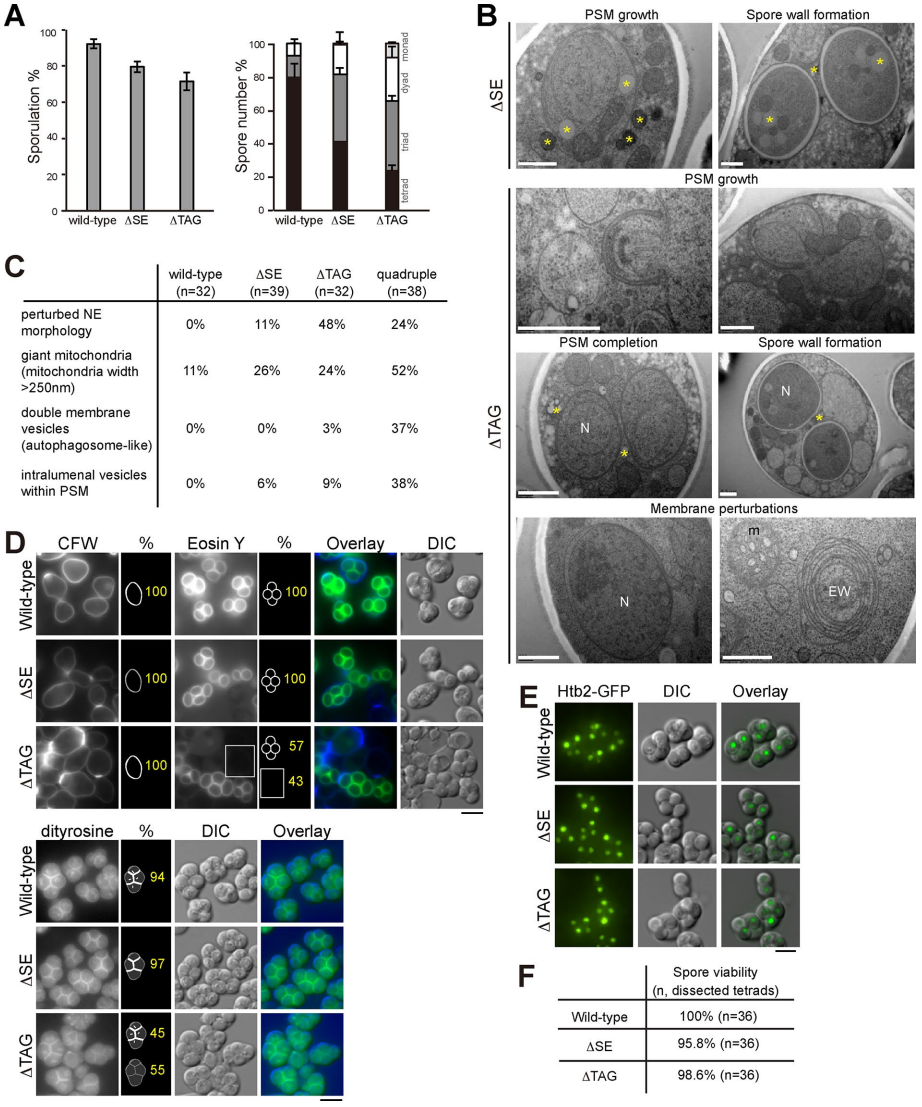

FIGURE 4: Evaluation of sporulation in cells lacking two major neutral lipids. (A) Left, percentage of indicated strains developing spores at 48 h after transferal to SPO. Right, number of spores formed in indicated mother cell ascus after 48 h in SPO. More than 200 cells were quantified, and the percentage is shown. ΔSE, *are1*Δ *are2*Δ; ΔTAG, *dga1*Δ *lro1*Δ. (B) Electron micrographs of the ΔSE and ΔTAG strains grown in SPO. Yellow asterisks, LDs. EW, ER whorl; m, mitochondria; N, nucleus. Scale bar, 0.5 µm. (C) Quantification of PSM and various membrane defects found during meiosis II, defined by cells harboring open PSM structures, in the EM results. *n* is the total number of cells quantified. (D) Cell strains, as indicated, were grown in SPO for 24 h and stained with CFW and eosin Y or with dityrosine, followed by fluorescence microscopy. Quantification data counted from >150 cells for representative images. Inset, cell without eosin Y fluorescence. Scale bar, 5 µm. (E) Cell strains, as indicated, expressing Htb2-GFP were grown in SPO for 24 h and subjected to fluorescence microscopy. Htb2-GFP is shown as the maximal projection image. Scale bar, 5 µm. (F) Spore viability test for the indicated strains based on tetrad dissection.

lacking various acyltransferases for TAG or SE production, grew similarly to the wild type on YPD (1% yeast extract, 2% peptone, 2% glucose) plates (Figure 7A). To avoid any adaptation or mitochondria problems, we always analyzed sporulation using fresh cells from frozen stocks and tested and confirmed that the cells were respiratory competent (not petite). However, <25% of the quadruple mutant cells eventually sporulated, whereas the majority (>75%) failed to form any morphologically detectable spores (Figure 7B). We also noticed that the number of spores found in the mother cell ascus of the LD-deficient strain declined from 24 to 72 h, harboring mostly monads in the ascus after 72 h in SPO, which is distinct from the wild type or other mutants in this study (Figure 7B). The spores formed in the LD-deficient quadruple mutant displayed increased CFW but reduced eosin Y staining, and the dityrosine fluorescence was absent or discontinuous, indicating a spore wall assembly defect (Figure 7C). Most strikingly, nearly all of the spores formed in the LD-deficient quadruple mutant were inviable (Figure 7D).

Because the defects in PSM biogenesis may account for disrupted spore wall and spore inviability, we next performed EM, using serial sectioning to closely examine ultrastructural details in the quadruple mutant. The quadruple mutant, like the ΔTAG and ΔSE mutants, often displayed an irregular internuclear membrane space and had giant mitochondria (Figures 4C and 8A). Occasionally, an ER proliferation structure termed the ER whorl was found in the quadruple mutant and ΔTAG mutants (Figures 4C and 8A). However, these membrane perturbations were probably not the major cause of spore inviability in the quadruple mutant because ΔTAG and ΔSE cells formed the PSM and spores ultrastructurally similar to those in the wild type (Figure 4). Of interest, the majority of the PSM in the quadruple mutant was irregular and often branched (Figures 8Ab and Supplemental Figure S3) and frequently accumulated intraluminal vesicles similar to that in *vps13*Δ mutant (Park and Neiman, 2012). In some cells, the PSM formed without attachment to the MOP, or it attached without linking to the nuclear envelope (Figure 8Ab and Supplemental Figure S3). In addition, we routinely observed spores that developed spore walls before the closure of the PSM and had inner and outer spore wall invaginations or protrusions. Thus the ultrastructural evidence clearly showed that cells without LDs had aberrant PSM organization, which may lead to dead spores.

We next performed time-course experiments and quantified Htb2-GFP distribution to learn about chromosome segregation in the LD-deficient mutant during sporulation. Htb2-GFP was seen as a single focus in both the wild type and quadruple mutant at 6 h in SPO (Figure 8B). At 10 h in SPO, most wild-type cells contain two to four Htb2-GFP foci with a small population of cells already forming spores. After 17 h in SPO, most wild-type cells formed spores, and each of the spores contained one Htb2-GFP focus. By contrast, the majority of quadruple mutants arrested as two to four mispositioned Htb2-GFP foci (mostly four) after 17 h without spore formation. In addition, a diffused Htb2-GFP signal was seen within some cells, particularly at later time points, which may suggest cell death. Thus we conclude that the majority of LD-deficient quadruple mutants entered but failed to complete normal meiosis II, a stage when the PSM forms and grows, leading to cell death.

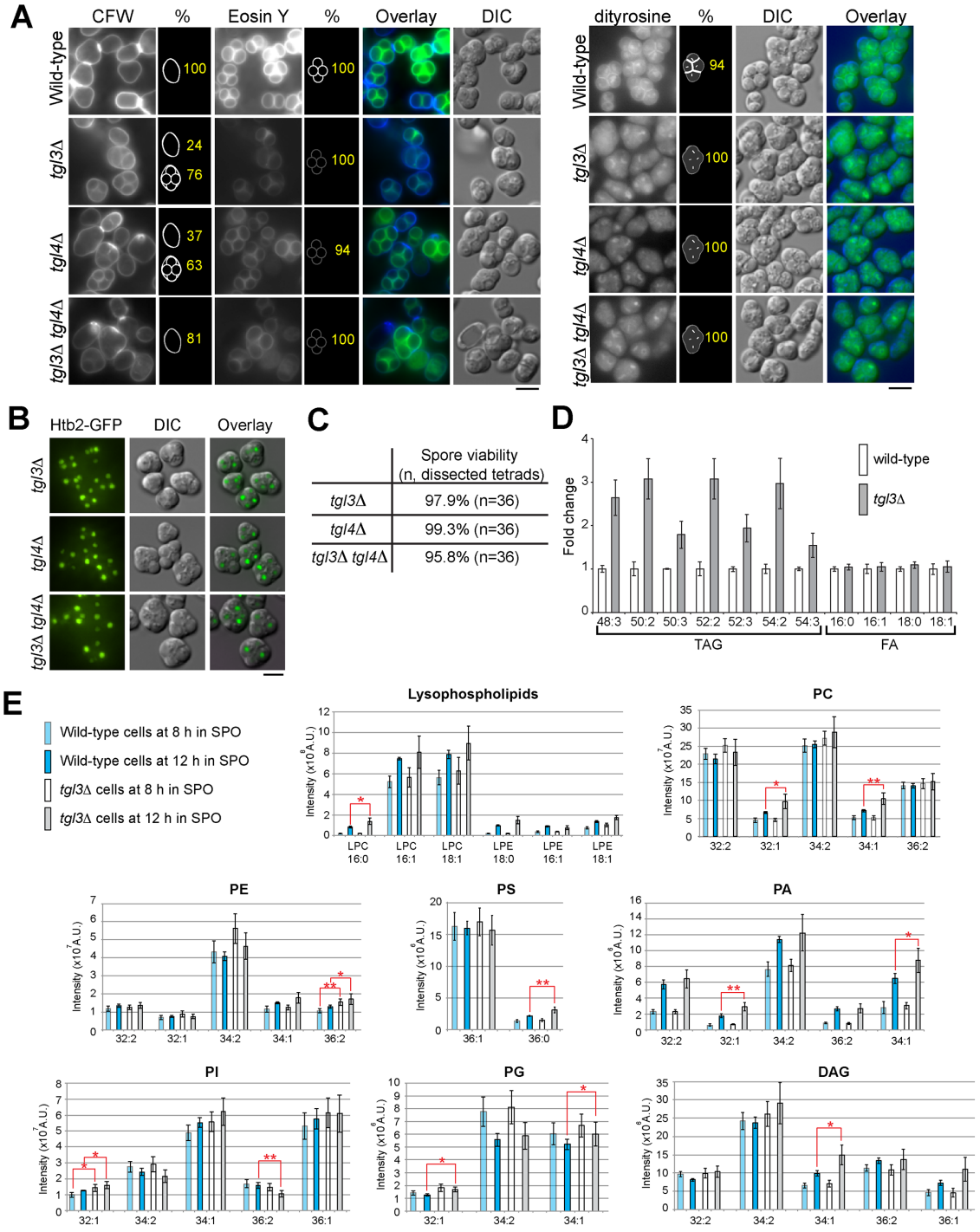

FIGURE 5: Evaluation of sporulation in cells lacking TAG lipases. (A) Cell strains, as indicated, were grown in SPO for 24 h and stained with CFW and eosin Y or with dityrosine, followed by fluorescence microscopy. Quantification data counted from >150 cells for representative images. Scale bar, 5 μm. (B) Cell strains, as indicated, expressing Htb2-GFP were grown in SPO for 24 h and subjected to fluorescence microscopy. Htb2-GFP is shown as the maximal projection image. Scale bar, 5 μm. (C) Spore viability test for the indicated strains based on tetrad dissection. (D) Lipids isolated from wild-type and *tgl3*Δ cells were analyzed by LC/MS. Fold change of indicated TAG and FA species relative to the level in wild type during 12 h in SPO is shown. The results are summarized from four independent experimental repeats and shown as mean ± SD. (E) Lipids isolated from wild-type and *tgl3*Δ cells harvested at the indicated time point were subjected to LC/MS. The intensity of indicated lipid species is quantified and plotted. The results are summarized from four independent experimental repeats and shown as mean ± SD. *$p < 0.05$; **$p < 0.01$.

To examine whether the abnormal meiosis II may be associated with spindle problems, we next followed the spindle marker GFP-Tub1 by a time-course experiment (Tsuchiya *et al.*, 2011). In wild-type cells, GFP-Tub1 mainly labeled SPB and appeared as single puncta at 6 h in SPO (Figure 8C), and the signal mostly appeared as single puncta within each of the spore in mother cell ascus after

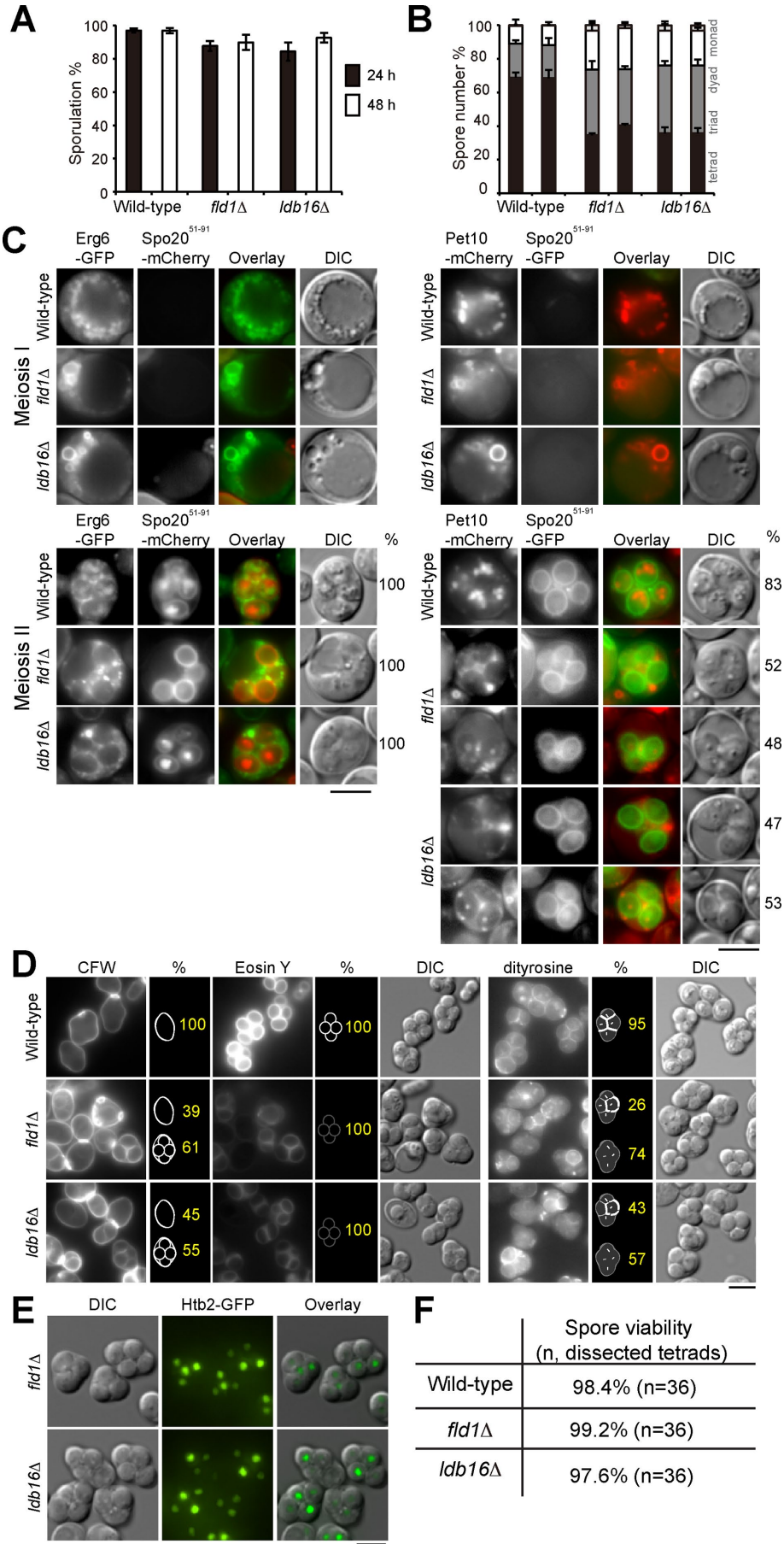

	Spore viability (n, dissected tetrads)
Wild-type	98.4% (n=36)
*fld1*Δ	99.2% (n=36)
*ldb16*Δ	97.6% (n=36)

17 h in SPO, indicating that meiosis II has completed. However, in the quadruple mutants, there were more duplicated SPB foci and meiotic spindles labeled with GFP-Tub1 at 11 and 14 h in SPO, indicative of slow or impaired progression through meiotic division. Most strikingly, GFP-Tub1 in the majority of quadruple mutants after 18 h in SPO appeared predominately as multiple small puncta or fragments, which may represent fragmented spindles (Figure 8C). Therefore the quadruple mutant likely suffers from impaired spindles, thereby failing to properly segregate the chromosomes, leading to cell death. Taking the results together, we conclude that the cellular organelle LDs is essential for yeast meiosis II progression. LDs and lipid homeostasis underlying LD physiology likely regulate both PSM growth and spindle organization to ensure proper chromosome segregation, enabling spore development and subsequent spore wall morphogenesis.

DISCUSSION

In this study, we addressed the dynamics and contribution of LDs during diploid yeast sporulation. We showed that LDs originally associated with the entire vacuole surface and then clustered near the dumbbell-shaped nucleus at the onset of meiosis II, when the PSM appeared (Figure 1). The change in LD distribution might be attributable to a reorganization of the LD–vacuole

FIGURE 6: Evaluation of sporulation in cells harboring LD assembly defects. (A) Percentage of wild-type, *fld1*Δ, and *ldb16*Δ cells developing spores at 24 and 48 h after transferal to SPO. (B) Number of spores formed in mother cell ascus after 24 (left) and 48 (right) h in SPO. More than 200 cells were quantified, and the percentage is shown. (C) Wild-type, *fld1*Δ, and *ldb16*Δ cells expressing Erg6-GFP and Spo20 (51-91)-mCherry or Pet10-mCherry and Spo20 (51-91)-GFP, as indicated, were imaged by fluorescence microscopy. Right, quantification data for the representative images during meiosis II. Scale bar, 5 μm. (D) Cell strains, as indicated, were grown in SPO for 24 h and stained with CFW and eosin Y or with dityrosine, followed by fluorescence microscopy. Quantification data for representative images. Scale bar, 5 μm. (E) Cell strains, as indicated, expressing Htb2-GFP were grown in SPO for 24 h and subjected to fluorescence microscopy. Htb2-GFP is shown as the maximal projection image. Scale bar, 5 μm. (F) Spore viability test based on tetrad dissection of wild-type, *fld1*Δ, and *ldb16*Δ cells.

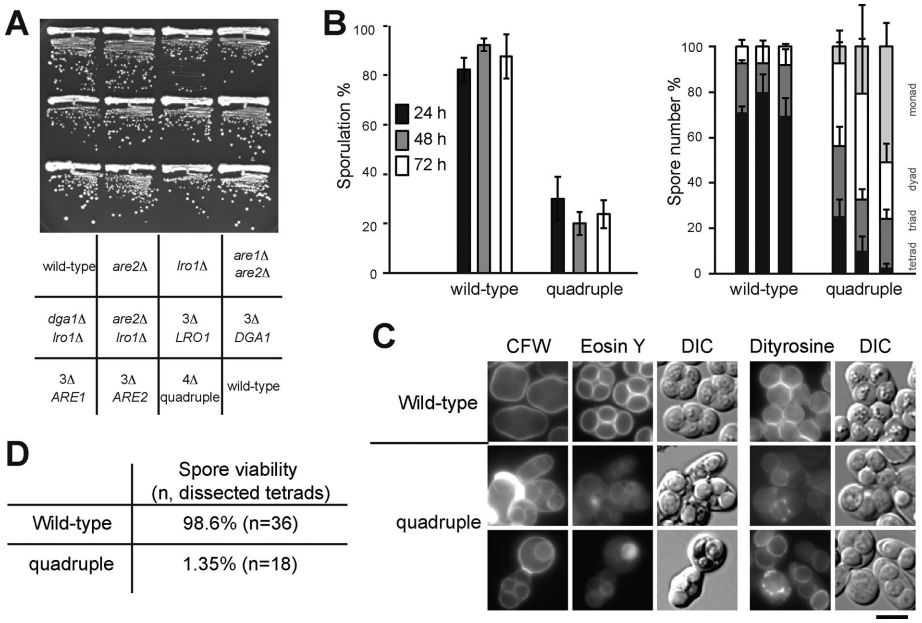

FIGURE 7: Severe sporulation defects in cells lacking LDs. (A) Growth of indicated strains on YPD plates incubated at 30°C for 2 d. (B) Left, percentage of wild-type and quadruple-mutant cells developing spores at 24, 48, and 72 h after transferal to SPO. Right, number of spores formed in the indicated mother cell ascus after (from left to right) 24, 48, and 72 h incubation in SPO. More than 200 cells were quantified for each strain, and the percentage is shown. (C) Wild-type and quadruple-mutant cells were grown in SPO for 24 h and subjected to CFW, eosin, and dityrosine staining, followed by fluorescence microscopy. (D) Spore viability test for the indicated strains based on tetrad dissection.

contact sites. Alternatively, LDs may be pulled away by vacuoles and/or the disassembly of the cortical ER (Suda *et al.*, 2007). Ultrastructural evidence indicated that docking of LDs to the PSM began when the precursor PSM was nucleated from the MOP by fusion of the dense core secretory vesicles and that LD structures shrunk as the PSM expanded (Figure 2). In addition, the shrinking LDs were often electron-dense in our ultrastructural analyses, which probably reflected a change in their lipid composition, such as an enrichment of FAs. Indeed, the notion that LD lipolysis during meiosis II promotes FA release is further supported by our sporulation lipidomic analyses (Figure 3).

To investigate the role of LD association with the PSM during meiosis II, we characterized several mutants affecting different aspects of LD physiology. We found that LD lipolysis and LD assembly defects correlated with the disrupted spore wall assembly (Figures 5 and 6), arguing that LD contents and/or their metabolites might regulate spore wall biosynthesis through lipolysis. LDs store predominantly two types of neutral lipids, TAG and SE. By characterizing ΔTAG and ΔSE mutants, we conclude that TAG but not SE is important for spore wall assembly (Figure 4). Though spore viability was not affected without either TAG or SE, spore development was drastically impaired when both were absent (Figure 7). The inviability of spores formed in the LD-deficient mutant may be attributed to at least two reasons (Figure 8). First, most PSM displayed abnormalities in the ultrastructure, including an unusually small size, formation of intraluminal vesicles, and failure in PSM closure, similar to the phenotype of *vps13*Δ. Second, the mutants also suffered from disrupted spindles, showing multiple puncta/fragments labeled with GFP-Tub1, during meiosis II progression.

The disrupted-spore-development phenotype in the LD-deficient mutant cannot be explained simply by a shortage of energy or membranes. Instead, we suggest that LDs are central for membrane morphogenesis during spore development. LDs likely contribute to this unique morphogenesis program through their highly dynamic localization pattern via contact with the vacuole first during meiosis I to eventually dock on the PSM during meiosis II. Given that the LD-deficient mutant displays a similar phenotype as *vps13*Δ, LDs may regulate Vps13 or Vps13-mediated processes. Although originally assigned a role in vesicular traffic, Vps13 is believed to promote PSM growth by regulating inositol phosphates and Spo14 PLD activity during sporulation, and the protein interacts with Spo71 to execute their functions on the PSM (Park and Neiman, 2012; Park *et al.*, 2013; Parodi *et al.*, 2012). Like Vps13, Spo71 might also function through lipids, as the protein genetically interacts with Spo1, which has homology with phospholipase B (Parodi *et al.*, 2012). *vps13*Δ mutants displayed reduced PI4,5-P2 and PI4-P levels, and the PSM formed in *vps13*Δ had a reduced PA levels (Park and Neiman, 2012). Consistently, the intensity of the PA indicator Spo20 (51-91)-GFP on the PSM in the LD-deficient strain was much weaker (unpublished data). Thus we suspect that PI4-P, PI4,5-P2, PA, and various other lipids were likely perturbed in the LD-deficient mutant. We suggest that the unique PSM morphogenesis function of LDs is likely attributable to its role in controlling lipid homeostasis/utilization.

TAG hydrolysis occurred during meiosis II, most likely through the contact of LDs with the PSM, with apparent shrinkage of LDs. Our lipodome revealed a striking increase of PA during sporulation (Figure 3C), which is consistent with previous studies showing that increased PLD activity is essential for sporulation (Rudge *et al.*, 1998; Nakanishi *et al.*, 2006). However, we did not detect a correlation of the reduction of PC with the same acyl chain length for the up-regulated PA during sporulation. Because PA is a low-abundance phospholipid, the high PC level might shield the effect of the previously established role of PLD to synthesize PA from PC. Our lipidome also identified selective storage and consumption of TAG harboring a longer acyl chain (Figure 3B). Besides supplying energy, released FAs may act as signaling molecules or be metabolized into phospholipids by acylation, and the unsaturated FAs enhance membrane fluidity. It was previously found that Tgl3 and Tgl5 catalyzed oleoyl-CoA–dependent acylation of lyso-PE and lyso-PA to form PE and PA, respectively, and that the acyltransferase, rather than the lipase, function of Tgl3 was crucial for sporulation (Rajakumari and Daum, 2010). Thus it is possible that LD surface lysophospholipids might be converted into phospholipids by these activities to promote PSM growth. However, we observed increase instead of decrease of several lysophospholipids and phospholipids with *tgl3*Δ. Thus how TAG lipolysis contributes to spore wall morphogenesis remains obscure. In addition, oleate released via lipolysis may exert other important functions for spore development. Yeast sporulation was inhibited by cerulenin, an inhibitor for FA synthesis, whereas addition of oleate or sporulated yeast extract rescued the defect (Ohno *et al.*, 1976). Increased oleate levels may induce expression

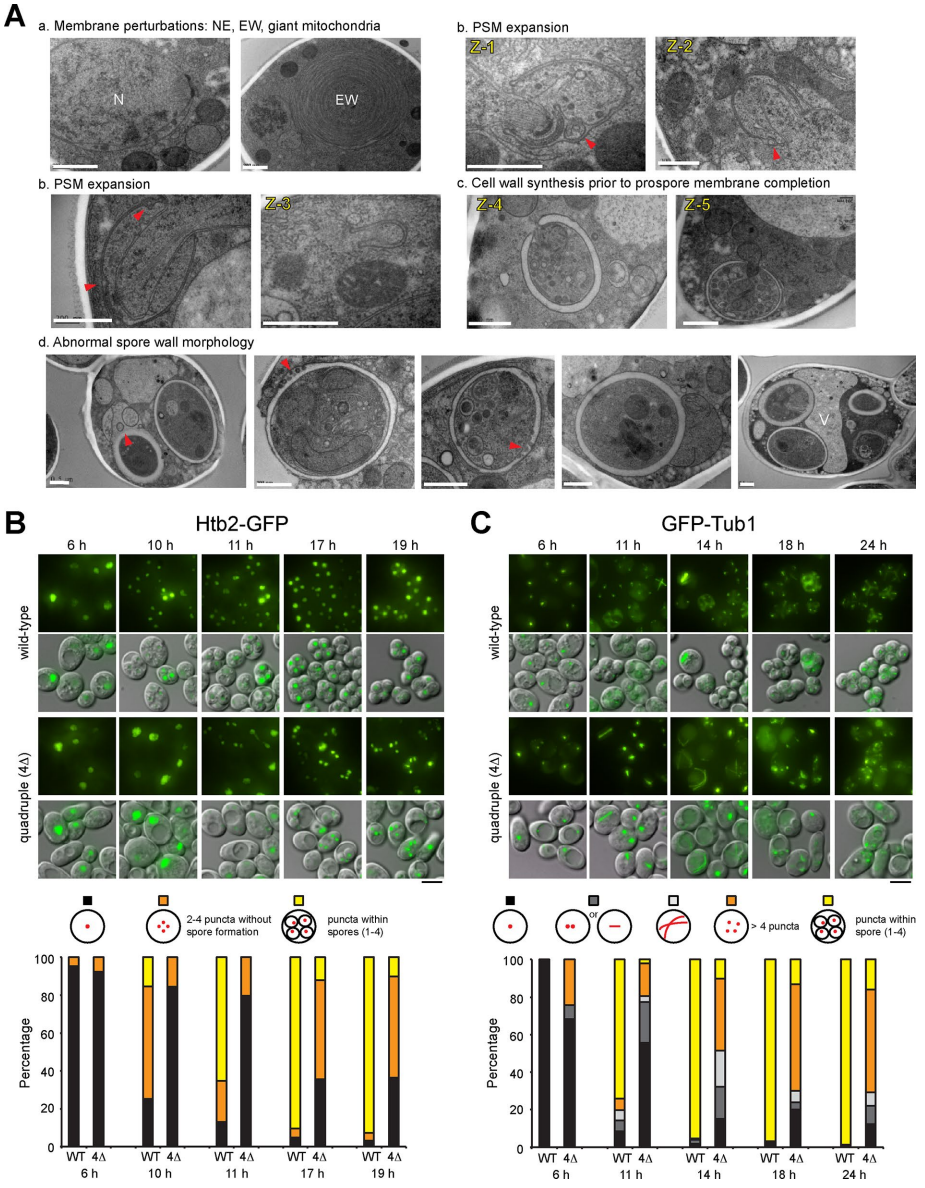

FIGURE 8: Defective PSM growth, chromosome segregation, and spindle organization in LD-deficient quadruple mutants undergoing meiosis II. (A) Electron micrographs of the quadruple mutant grown in SPO. Serial sectioning of images Z-1 to Z-5 is shown in Supplemental Figure S3. Red arrowheads denote intraluminal vesicles. Scale bar, 0.5 μm. (B) Htb2-GFP localization in diploid yeast cells grown in SPO at the indicated time points. In addition to the representative images, the population of cells displaying the indicated Htb2-GFP pattern was quantified, and the percentage is plotted. More than 200 cells were counted at each time point. (C) Same as B, except that GFP-Tub1 is shown.

of genes needed for sporulation, such as *SPS19* (Gurvitz *et al.*, 1997, 1999). Oleate may regulate lipid enzyme activities. For example, the key lipid-remodeling enzyme PLD was stimulated by oleate in *Schizosaccharomyces pombe* (Harkins *et al.*, 2010). However, the PLD Spo14 in *S. cerevisiae* was affected by PI4,5-P2 but not by oleate.

The cytological and physiological evidence led us to propose that lipolysis of LDs is activated upon docking on the PSM by signaling molecules and influences PSM growth. The yeast perilipin-like protein Sps4 is induced in sporulation (Garber and Segall, 1986), probably regulating lipolysis as its mammalian counterpart. It is conceivable that lipid remodeling occurs during yeast sporulation; however, it remains to be determined whether certain types of lipids are required for spore development. In this study, we provide the first lipidome for yeast sporulation and identified many lipid species whose levels are affected during different meiosis stages (Figure 3C). Understanding their roles and the contributions of various lipid enzymes to their synthesis or modification will provide further insights into the mysterious process of de novo PSM morphogenesis. The yeast sporulation model will provide further insights into our knowledge on lipolysis.

MATERIALS AND METHODS

Strains, growth conditions, and reagents

Yeast strains and plasmids used in this study are listed in Supplemental Table S1. Haploid yeast strains were generated by tetrad dissection or using a PCR-based transformation approach (Longtine *et al.*, 1998). Transformants were selected on synthetic complete with dextrose (SCD)-dropout medium at 30°C, and the integration of genes was further confirmed by colony PCR. Haploid strains of two mating types were mated to generate diploid strains. Sporulation condition refers to cells that were grown on either YPD or SCD–Ura+CA (0.67% yeast nitrogen base, complete amino acids without uracil, 2% glucose, and 0.2% casamino acids) plates for 3–4 d and subjected directly to CSH SPO medium (1% KOAc, 0.1% yeast extract, 0.05% glucose) with a starting OD_{600} of ~2.0. BODIPY 493/503 was from Thermo Fisher Scientific (Waltham, MA), osmium tetraoxide and Spurr were from Electron Microscopy Sciences (Hatfield, PA), uranyl acetate was from SPI-CHEM (West Chester, PA), and acetone was from Merck (Kenilworth, NJ). All other reagents were from Sigma-Aldrich (St. Louis, MO).

Live microscopy and image processing

To image sporulating yeast cells by time-lapse microscopy, cells were stained with BODIPY 493/503 and loaded into a CellAsic chamber Y04 plate (Merck Millipore, Darmstadt, Germany). Images were acquired at 30°C with a Plan Apochromat 100× objective lens and a live set filter for GFP (525/50 nm) and mCherry (632/60 nm), which were controlled by the DeltaVision system (GE Healthcare) equipped with a CoolSNAP HQ2 charge-coupled device (CCD) camera (Photometrics) and softWoRx suite software (GE Healthcare). For still image acquisition, we used an Olympus IX81 microscope equipped with a Plan Apochromat 100× lens, CoolSNAP HQ2 CCD camera, and analySIS software (Olympus, Tokyo, Japan). To determine HTB2-GFP and GFP-Tub1 distribution in the mother cell ascus, we used an Olympus IX81 microscope equipped with a Plan Apochromat 100× lens, ORCA-Flash 4.0 cMOS V2 camera (Hamamatsu), and MetaMorph software (Molecular Devices) to image cells with eight

Z-sections with a spacing of 1 µm and subsequent maximal projection. We used 488-nm excitation with a bandpass 500- to 530-nm filter to detect GFP, a 561-nm excitation with a band pass 575- to 630-nm filter for mCherry, and 372-nm excitation and 456-nm emission filters for 4′,6-diamidino-2-phenylindole (DAPI)/blue fluorescent protein (BFP). Images were processed by MetaMorph, ImageJ (National Institutes of Health, Bethesda, MD), or Photoshop (CS4; Adobe, San Jose, CA).

Electron microscopy

Yeast cells were grown under conditions described earlier. Cells (~10 OD_{600} units) were centrifuged and immediately subjected to cryofixation by high-pressure freezing (High Pressure Freezer EM HPM100; Leica, Wetzlar, Germany), followed by freeze substitution and low-temperature embedding (EM AFS2; Leica). Freeze substitution was performed in 2% osmium tetroxide and 0.1% uranyl acetate in acetone at –85°C for 66 h, –50°C for 10 h, –20°C for 10 h, and 0°C for 6 h, with the temperature increased 5°C/h between steps. The samples were then washed in acetone and subjected to infiltration with 5, 10, 25, 50, 75, and 100% Spurr resin. After polymerization at 70°C for 48 h, the blocks were cut into 70- to 90-nm ultrathin sections on the ultramicrotome (EM UC6; Leica) with a diamond knife (Ultra 45°, DiATOME; Biel, Switzerland). Sections were placed on 0.4% Formvar-coated slot grids (EMS) and imaged at 120 kV on a transmission electron microscope (Tecnai G2 Spirit TWIN; FEI, Hillsboro, OR) using a digital CCD camera (832 Orius SC1000B; Gatan, Pleasanton, CA). The images were processed with Photoshop software (CS4; Adobe).

Cell wall (CFW, eosin Y, and dityrosine) and LD staining

The procedure for CFW, eosin Y, and dityrosine staining was previously described (Lin *et al.*, 2013). In brief, 500 µl cells of incubated in CSH SPO for 1 d were harvested and washed with McIlvanice buffer (citrate phosphate buffer, pH 4.0), and 1 µl of CFW (1 mg/ml) and 15 µl of eosin Y (10 mg/ml) were used to stain the cell in the dark for 10 min. After being washed, cells were immediately visualized by fluorescence microscopy. CFW staining was imaged with a DAPI filter and eosin Y with a GFP filter. To detect dityrosine fluorescence, we harvested and washed 500 µl of sporulating cells with water, followed by incubation in 1 ml of 0.1 M NaOH for fluorescence microscopy using a DAPI filter. To stain LDs, 5 µl of 0.5 mg/ml BODIPY 493/503 was added to 500 µl of sporulating yeast cells to stain LDs in the dark for 10 min, followed by two washes with 50 mM Tris, pH 7.5.

Quantification of yeast sporulation

Diploid yeast cell shifted to CSH SPO medium for 24, 48, or 72 h were imaged by differential interference contrast microscopy. At least 200 cells were manually grouped, based on the number of spores formed in the mother cell ascus. Sporulation efficiency was defined as the percentage of cells that form spores, regardless of the number of spores, relative to the total number of cells counted. Spore type was quantified and plotted as the number of spores accumulated in the mother cell ascus. Data are displayed as mean ± SD from three independent experiments. We dissected 16–18 tetrads from 24-h cultures and another 16–18 tetrads from 48-h cultures. The viability of spores was based on the sum of the viable spores on YPD from a total of ~36 tetrads from 24- and 48-h cultures. Because of greatly reduced sporulation rates and difficulties in manipulation, we dissected only ~18 tetrads for LD-deficient quadruple mutants.

Lipid analyses

Lipid extraction was performed as previously described (Folch *et al.*, 1957). Briefly, 40 OD_{600} units of cells were collected and lysed by bead beating in methanol, and then chloroform was added. Linoleic acid-d4 (Cayman Chemical, Ann Arbor, MI) or heptadecanoic acid (Sigma-Aldrich) and d5-TG ISTD Mix (Avanti) was added before the bead-beating step to serve as an internal standard for subsequent lipid quantification. The samples were centrifuged to remove debris and the supernatants supplemented with sodium chloride. After centrifugation, the aqueous phase was removed from the top, and the organic phase, containing lipids, was dried with a SpeedVac (Thermo Scientific, Waltham, MA). The lipids were then dissolved in chloroform:methanol (2:1). For lipid profiling, we used a linear ion trap-Orbitrap mass spectrometer (Orbitrap Elite; Thermo Fisher Scientific) coupled online with an ultrahigh-performance LC system (ACQUITY UPLC; Waters, MA). We used solvent A with 10 mM ammonium acetate, pH 5.0, and 40% acetonitrile in the aqueous phase and solvent B with 10 mM ammonium acetate, pH 5.0, and 10% acetonitrile in isopropyl alcohol in the mobile phase for LC separation. The lipids were separated online with a reversed-phase column (CSH C18, 1.8 µm, 2.1 mm × 100 mm, Waters) at a flow rate of 450 µl/min using a gradient of 40–99.5% solvent B over 0–10 min. The total chromatography separation time for each analysis was 14 min. The mass spectrometer was operated in positive- and negative-ion modes and set to one full Fourier transform MS scan (m/z = 100–1200, resolution = 30,000). The lipids were quantified with Xcalibur software (Thermo Scientific) followed by analysis with Excel (Microsoft).

ACKNOWLEDGMENTS

We are grateful to Ji-Ying Huang and Mei-Jane Fang at the Live-Cell Imaging Core Laboratory (Institute of Plant and Microbial Biology, Academia Sinica) for microscopy assistance, Yu-Ching Wu at the Small Molecule Metabolomics Core Laboratory (Institute of Plant and Microbial Biology) for advice on lipidomic analysis, members of the Institute of Plant and Microbial Biology, Institute of Molecular Biology, and Institute of Cellular and Organistic Biology EM core facilities for helpful discussions, and former Wang lab members Yi-Shun Chang, Chia-Yin Huang, and Tze-Yu Tsao for technical assistance. This work was supported by grants from the Ministry of Science and Technology (104-2311-B-001-015-MY3 and 104-2633-B-001-001 to C.-W.W.) and Academia Sinica (intramural funds and Career Development Award to C.-W.W.).

REFERENCES

Coluccio A, Bogengruber E, Conrad MN, Dresser ME, Briza P, Neiman AM (2004). Morphogenetic pathway of spore wall assembly in Saccharomyces cerevisiae. Eukaryot Cell 3, 1464–1475.

Diamond AE, Park JS, Inoue I, Tachikawa H, Neiman AM (2009). The anaphase promoting complex targeting subunit Ama1 links meiotic exit to cytokinesis during sporulation in Saccharomyces cerevisiae. Mol Biol Cell 20, 134–145.

Eastwood MD, Meneghini MD (2015). Developmental coordination of gamete differentiation with programmed cell death in sporulating yeast. Eukaryot Cell 14, 858–867.

Fares H, Goetsch L, Pringle JR (1996). Identification of a developmentally regulated septin and involvement of the septins in spore formation in Saccharomyces cerevisiae. J Cell Biol 132, 399–411.

Fei W, Shui G, Gaeta B, Du X, Kuerschner L, Li P, Brown AJ, Wenk MR, Parton RG, Yang H (2008). Fld1p, a functional homologue of human seipin, regulates the size of lipid droplets in yeast. J Cell Biol 180, 473–482.

Folch J, Lees M, Sloane Stanley GH (1957). A simple method for the isolation and purification of total lipides from animal tissues. J Biol Chem 226, 497–509.

Garber AT, Segall J (1986). The Sps4-gene of Saccharomyces-cerevisiae encodes a major sporulation-specific messenger-RNA. Mol Cell Biol 6, 4478–4485.

Grippa A, Buxo L, Mora G, Funaya C, Idrissi FZ, Mancuso F, Gomez R, Muntanya J, Sabido E, Carvalho P (2015). The seipin complex Fld1/Ldb16 stabilizes ER-lipid droplet contact sites. J Cell Biol 211, 829–844.
Gurvitz A, Hamilton B, Hartig A, Ruis H, Dawes IW, Rottensteiner H (1999). A novel element in the promoter of the Saccharomyces cerevisiae gene SPS19 enhances ORE-dependent up-regulation in oleic acid and is essential for derepression. Mol Gen Genet 262, 481–492.
Gurvitz A, Rottensteiner H, Hiltunen JK, Binder M, Dawes IW, Ruis H, Hamilton B (1997). Regulation of the yeast SPS19 gene encoding peroxisomal 2,4-dienoyl-CoA reductase by the transcription factors Pip2p and Oaf1p: beta-oxidation is dispensable for Saccharomyces cerevisiae sporulation in acetate medium. Mol Microbiol 26, 675–685.
Guth E, Hashimoto T, Conti SF (1972). Morphogenesis of ascospores in Saccharomyces cerevisiae. J Bacteriol 109, 869–880.
Harkins AL, Yuan G, London SD, Dolan JW (2010). An oleate-stimulated, phosphatidylinositol 4,5-bisphosphate-independent phospholipase D in Schizosaccharomyces pombe. FEMS Yeast Res 10, 717–726.
Jacquier N, Choudhary V, Mari M, Toulmay A, Reggiori F, Schneiter R (2011). Lipid droplets are functionally connected to the endoplasmic reticulum in Saccharomyces cerevisiae. J Cell Sci 124, 2424–2437.
Klis FM, Mol P, Hellingwerf K, Brul S (2002). Dynamics of cell wall structure in Saccharomyces cerevisiae. FEMS Microbiol Rev 26, 239–256.
Knop M, Strasser K (2000). Role of the spindle pole body of yeast in mediating assembly of the prospore membrane during meiosis. EMBO J 19, 3657–3667.
Lesage G, Bussey H (2006). Cell wall assembly in Saccharomyces cerevisiae. Microbiol Mol Biol Rev 70, 317–343.
Lin CP, Kim C, Smith SO, Neiman AM (2013). A highly redundant gene network controls assembly of the outer spore wall in S. cerevisiae. PLoS Genet 9, e1003700.
Longtine MS, McKenzie A 3rd, Demarini DJ, Shah NG, Wach A, Brachat A, Philippsen P, Pringle JR (1998). Additional modules for versatile and economical PCR-based gene deletion and modification in Saccharomyces cerevisiae. Yeast 14, 953–961.
Lynn RR, Magee PT (1970). Development of the spore wall during ascospore formation in Saccharomyces cerevisiae. J Cell Biol 44, 688–692.
Maier P, Rathfelder N, Finkbeiner MG, Taxis C, Mazza M, Le Panse S, Haguenauer-Tsapis R, Knop M (2007). Cytokinesis in yeast meiosis depends on the regulated removal of Ssp1p from the prospore membrane. EMBO J 26, 1843–1852.
Moens PB, Rapport E (1971). Spindles, spindle plaques, and meiosis in the yeast Saccharomyces cerevisiae (Hansen). J Cell Biol 50, 344–361.
Moreno-Borchart AC, Strasser K, Finkbeiner MG, Shevchenko A, Shevchenko A, Knop M (2001). Prospore membrane formation linked to the leading edge protein (LEP) coat assembly. EMBO J 20, 6946–6957.
Nakanishi H, de los Santos P, Neiman AM (2004). Positive and negative regulation of a SNARE protein by control of intracellular localization. Mol Biol Cell 15, 1802–1815.
Nakanishi H, Morishita M, Schwartz CL, Coluccio A, Engebrecht J, Neiman AM (2006). Phospholipase D and the SNARE Sso1p are necessary for vesicle fusion during sporulation in yeast. J Cell Sci 119, 1406–1415.
Neiman AM (1998). Prospore membrane formation defines a developmentally regulated branch of the secretory pathway in yeast. J Cell Biol 140, 29–37.
Neiman AM (2011). Sporulation in the budding yeast Saccharomyces cerevisiae. Genetics 189, 737–765.
Ohno T, Awaya J, Omura S (1976). Inhibition of sporulation by cerulenin and its reversion by exogenous fatty acids in Saccharomyces cerevisiae. Antimicrob Agents Chemother 9, 42–48.
Park JS, Neiman AM (2012). VPS13 regulates membrane morphogenesis during sporulation in Saccharomyces cerevisiae. J Cell Sci 125, 3004–3011.
Park JS, Okumura Y, Tachikawa H, Neiman AM (2013). SPO71 encodes a developmental stage-specific partner for Vps13 in Saccharomyces cerevisiae. Eukaryot Cell 12, 1530–1537.
Parodi EM, Baker CS, Tetzlaff C, Villahermosa S, Huang LS (2012). SPO71 mediates prospore membrane size and maturation in Saccharomyces cerevisiae. Eukaryot Cell 11, 1191–1200.
Rajakumari S, Daum G (2010). Janus-faced enzymes yeast Tgl3p and Tgl5p catalyze lipase and acyltransferase reactions. Mol Biol Cell 21, 501–510.
Ren J, Pei-Chen Lin C, Pathak MC, Temple BR, Nile AH, Mousley CJ, Duncan MC, Eckert DM, Leiker TJ, Ivanova PT, *et al.* (2014). A phosphatidylinositol transfer protein integrates phosphoinositide signaling with lipid droplet metabolism to regulate a developmental program of nutrient stress-induced membrane biogenesis. Mol Biol Cell 25, 712–727.
Riedel CG, Mazza M, Maier P, Korner R, Knop M (2005). Differential requirement for phospholipase D/Spo14 and its novel interactor Sma1 for regulation of exocytotic vesicle fusion in yeast meiosis. J Biol Chem 280, 37846–37852.
Rose K, Rudge SA, Frohman MA, Morris AJ, Engebrecht J (1995). Phospholipase D signaling is essential for meiosis. Proc Natl Acad Sci USA 92, 12151–12155.
Rudge SA, Morris AJ, Engebrecht J (1998). Relocalization of phospholipase D activity mediates membrane formation during meiosis. J Cell Biol 140, 81–90.
Rudge SA, Sciorra VA, Iwamoto M, Zhou C, Strahl T, Morris AJ, Thorner J, Engebrecht J (2004). Roles of phosphoinositides and of Spo14p (phospholipase D)-generated phosphatidic acid during yeast sporulation. Mol Biol Cell 15, 207–218.
Sciorra VA, Rudge SA, Prestwich GD, Frohman MA, Engebrecht J, Morris AJ (1999). Identification of a phosphoinositide binding motif that mediates activation of mammalian and yeast phospholipase D isoenzymes. EMBO J 18, 5911–5921.
Suda Y, Nakanishi H, Mathieson EM, Neiman AM (2007). Alternative modes of organellar segregation during sporulation in Saccharomyces cerevisiae. Eukaryot Cell 6, 2009–2017.
Szymanski KM, Binns D, Bartz R, Grishin NV, Li WP, Agarwal AK, Garg A, Anderson RG, Goodman JM (2007). The lipodystrophy protein seipin is found at endoplasmic reticulum lipid droplet junctions and is important for droplet morphology. Proc Natl Acad Sci USA 104, 20890–20895.
Tachikawa H, Bloecher A, Tatchell K, Neiman AM (2001). A Gip1p-Glc7p phosphatase complex regulates septin organization and spore wall formation. J Cell Biol 155, 797–808.
Tsuchiya D, Gonzalez C, Lacefield S (2011). The spindle checkpoint protein Mad2 regulates APC/C activity during prometaphase and metaphase of meiosis I in Saccharomyces cerevisiae. Mol Biol Cell 22, 2848–2861.
Walther TC, Farese RV Jr (2012). Lipid droplets and cellular lipid metabolism. Annu Rev Biochem 81, 687–714.
Wang CW (2015). Lipid droplet dynamics in budding yeast. Cell Mol Life Sci 72, 2677–2695.
Wang CW, Miao YH, Chang YS (2014a). Control of lipid droplet size in budding yeast requires the collaboration between Fld1 and Ldb16. J Cell Sci 127, 1214–1228.
Wang CW, Miao YH, Chang YS (2014b). A sterol-enriched vacuolar microdomain mediates stationary phase lipophagy in budding yeast. J Cell Biol 206, 357–366.